



## A highly stretchable smart dressing for wound infection monitoring and treatment

Rui Su<sup>a,b,1</sup>, Liangliang Wang<sup>a,1</sup>, Fei Han<sup>c</sup>, Shaoquan Bian<sup>a</sup>, Fengzhen Meng<sup>a</sup>, Weichen Qi<sup>d</sup>, Xinyun Zhai<sup>e</sup>, Hanfei Li<sup>c</sup>, Jun Wu<sup>f</sup>, Xiaohua Pan<sup>g</sup>, Haobo Pan<sup>a</sup>, Peizhi Guo<sup>b</sup>, William W. Lu<sup>d,h</sup>, Zhiyuan Liu<sup>c,i,\*</sup>, Xiaoli Zhao<sup>a,\*\*</sup>

<sup>a</sup> Research Center for Human Tissue and Organs Degeneration, Institute of Biomedicine and Biotechnology, Shenzhen Institute of Advanced Technology, Chinese Academy of Sciences, Shenzhen 518055, China

<sup>b</sup> Institute of Materials for Energy and Environment, State Key Laboratory of Bio-fibers and Eco-textiles, School of Materials Science and Engineering, Qingdao University, Qingdao 266071, China

<sup>c</sup> Neural Engineering Center, Shenzhen Institute of Advanced Technology, Chinese Academy of Sciences, Shenzhen 518000, China

<sup>d</sup> Department of Orthopaedics and Traumatology, The University of Hong Kong, Hong Kong 999077, China

<sup>e</sup> Center for Rare Earth and Inorganic Functional Materials, School of Materials Science and Engineering, National Institute for Advanced Materials, Nankai University, Tianjin 300350, China

<sup>f</sup> Shenzhen Key Laboratory for Innovative Technology in Orthopaedic Trauma, The University of Hong Kong-Shenzhen Hospital, Shenzhen 518053, China

<sup>g</sup> Southern Medical University, Shenzhen Bao'an People's Hospital, Dept Orthoped & Traumatol, Shenzhen 518101, China

<sup>h</sup> Department of Pharmaceutical Materials and Translational Medicine, Faculty of Pharmaceutical Sciences, Shenzhen University of Advanced Technology, Shenzhen 518083, China

<sup>i</sup> Standard Robots Co., Ltd, Room 405, Building D, Huafeng International Robot Fusen Industrial Park, Hangcheng Avenue, Guxing Community, Xixiang Street, Baoan District, Shenzhen, 518055, China

### ARTICLE INFO

#### Keywords:

Liquid metal  
Highly stretchable electronics  
Smart wound dressing  
Wound infection monitoring  
Electrically controlled drug delivery

### ABSTRACT

Smart dressings integrated with bioelectronics have attracted considerable attention and become promising solutions for skin wound management. However, due to the mechanical distinction between human body and the interface of electronics, previous smart dressings often suffered obvious degradation in electrical performance when attached to the soft and curvilinear wound sites. Here, we report a stretchable dressing integrated with temperature and pH sensor for wound status monitoring, as well as an electrically controlled drug delivery system for infection treatment. The wound dressing was featured with the deployment of liquid metal for seamless connection between rigid electrical components and gold particle-based electrodes, achieving a stretchable soft-hard interface. Stretching tests showed that both the sensing system and drug delivery system exhibited good stretchability and long-term stable conductivity with the resistance change rate less than 6 % under 50 % strain. Animal experiments demonstrated that the smart dressing was capable of detecting bacterial infection via the biomarkers of temperature and pH value and the infection factors of wound were significantly improved with therapy through electrically controlled antibiotics releasing. This proof-of-concept prototype has potential to significantly improve management of the wound, especially those with dynamic strain.

### 1. Introduction

Wound healing process normally undergoes four stages of coagulation, inflammation, proliferation and remodelling [1,2]. The

inflammatory stage is prone to bacterial infection, which greatly delays the wound healing process. Therefore, early symptomatic treatment of infection is crucial to accelerate wound healing and relieve the patient's pain. Traditionally, skin wounds are covered with dressings to provide a

\* Corresponding author. Neural Engineering Center, Shenzhen Institute of Advanced Technology, Chinese Academy of Sciences, Shenzhen 518055, China.

\*\* Corresponding author. Research Center for Human Tissue and Organs Degeneration, Institute of Biomedicine and Biotechnology, Shenzhen Institute of Advanced Technology, Chinese Academy of Sciences, Shenzhen 518055, China.

E-mail addresses: [zy.liu1@siat.ac.cn](mailto:zy.liu1@siat.ac.cn) (Z. Liu), [zhao.xl@siat.ac.cn](mailto:zhao.xl@siat.ac.cn) (X. Zhao).

<sup>1</sup> These authors contributed equally to this work.

<https://doi.org/10.1016/j.mtbio.2024.101107>

Received 9 January 2024; Received in revised form 23 May 2024; Accepted 31 May 2024

Available online 31 May 2024

2590-0064/© 2024 Published by Elsevier Ltd. This is an open access article under the CC BY-NC-ND license (<http://creativecommons.org/licenses/by-nc-nd/4.0/>).

protection against the external environment and promote healing [3,4]. But such medical measure has poor timeliness, thus appropriate monitoring equipment is needed to timely feedback changes of wound status. In addition, wound infection requires frequent dressing changes and medication, which brings more pain to the patient [5–7]. Therefore, a close-loop treatment system is also required for improving wound management and bringing better clinical outcomes [8].

Recent advances in flexible electronics enable wound dressings to integrate with biosensing and active treatment system [9–13]. Such smart dressings can detect the wound infection and accelerate wound healing. Wound infection can cause changes in some physiological parameters, like pH, temperature and other chemical factors. The increase in temperature is due to the increase of inflammatory factors and the dilation of capillaries caused by infection [14,15]. Based on this, Lou et al. created a flexible wound healing system integrated with miniaturized temperature sensor, which was able to monitor the wound regeneration process and provide early warning of infection [16]. Pang et al. also reported a smart flexible wound dressing that is capable of monitoring wound temperature as the early predictor of infection. Notably, UV-LEDs were integrated into their system for on-demand treatment by dynamic antibiotics releasing [17]. Recent studies have made great efforts in multiplex sensing of biomarkers to obtain more accurate diagnosis of the wound status. For optimal monitoring of wound infection, Jiang et al. chose to integrate a smart bandage with a thermistor and a skin impedance sensor to predict inflammatory states [18]. Most recently, a panel of biomarkers including temperature, pH, ammonium, glucose, lactate, and UA was considered for reflecting the infection, metabolic, and inflammatory status of chronic wounds [19]. However, integration of such multiplex sensing system into the wound dressing was very challenging. In practice, it has been demonstrated that wound pH and temperature were the most typical and effective biomarkers for providing information about wound conditions [20–24].

Irrespective of the fact that smart wound dressings advanced rapidly, especially in biomarker sensing and active wound treatment, there are still some obstacles to overcome in the development of these wearable electronics. A major challenge lies in the mechanical mismatch between human body and electrical components [25]. Traditionally, components such as transistors, sensors, and interconnects are constructed by rigid materials with high Young's moduli ( $>10^{10}$  Pa), whereas human skin have much lower moduli ( $<10^6$  Pa) [26]. In addition, previous studies show that body movements usually cause skin surfaces to stretch up to around 30 % strain [27,28]. The mechanical distinction and dynamic wound strain often lead to obvious degradation in the performance of the devices. To guarantee for accurate wound status monitoring and curative effect, the smart dressings should be made of stretchable materials that conformally integrate with curvilinear wounds under complex dynamic strains.

Conductive hydrogel has been extensively studied as wearable electronic devices in recent years for its softness and flexibility in minimizing the mechanical mismatch with biological tissue. However, further advances in conductive hydrogels with excellent mechanical properties and tissue adhesion are urgently needed [29]. Other than making breakthroughs in materials innovations, the most commonly used methods leverage readily available materials for achieving device stretchability. One of these strategies involves designing of flexible structures such as waves, origami, kirigami, and serpentine patterns using rigid conductive materials [30]. However, these flexible structures may suffer fatigue failure due to the movements of body parts. Another approach involves incorporating conductive fillers, such as metallic or carbon-based materials, onto or inside elastomers based on soft materials, including polydimethylsiloxane (PDMS) [31,32], Eco-flex [33,34], etc. But most of the conductive fillers are intrinsically solid with high Young's modulus. Large dynamic strain would cause aggregation of the solid conductive composites around the interface, resulting in electrical properties changes even deactivation of the device. Unlike solid conductive fillers, liquid metal has high electrical conductivity yet

extreme softness with very low Young's modulus, making them an attractive candidate for building stretchable electrodes [35–38]. Liquid metal could remain in a liquid state even under mechanical disruptions at room temperature, allowing conformal contact to irregular curvatures while maintaining electrical conductivity under deformation or stretching.

In this work, leveraging the excellent electrical conductivity and liquid-state deformability of the liquid metal, we developed a stretchable wound dressing for wound infection monitoring and on-demand drug delivery. Fig. 1A shows the application scenario of the stretchable wound dressing. Specifically, the dressing is a dedicatedly designed three-layer patch, including a Ecoflex based substrate, soft integrated circuit layer, and an ultra-thin encapsulation layer. The soft integrated circuit layer contains multiple sets of gold particle based soft electrodes for dual-channel sensing of wound temperature and pH value, as well as an electrically controlled antibiotics releasing system to combat wound infection. To ensure stable conductivity and efficient signal exchange under dynamic strain, liquid metal is introduced and encapsulated as the interconnections between the electrodes and rigid sensor or pins on the controller board. Combining the soft substrate and liquid metal-based interconnects, both the sensing system and drug delivery system exhibit good stretchability and long-term stable conductivity. Animal experiments demonstrated that the smart dressing was capable of detecting bacterial infection via the biomarkers of temperature and pH value and the infection factors of wound were significantly improved with therapy through electrically controlled antibiotics releasing.

## 2. Material and methods

### 2.1. Materials

The Ag/AgCl paste sourced from ALS Co., Ltd. (Japan) was used for building the reference electrodes. Aniline, KCl, HCl, and  $H_2SO_4$  were obtained from the Sinopharm group. Ecoflex 0020 was obtained from Smooth-On (America). The acrylic plate was bought from Shengjili (Shenzhen), liquid metal (Gallium indium alloy, 11 °C) from HuaTai (Shenzhen). Aladdin provided the phosphate buffered saline (PBS; pH = 7.2–7.4). Cefazoline sodium, polypyrrole, etc. were obtained from Innochem. The pH buffer (pH 4–9) was bought from Concord Technology (Tianjin). LiChuang (Shenzhen) supplied the thermistor 0805 and the FPC. In all the experiments, deionized water (DI) and Millipore water were employed. All chemicals were used in the experiments upon arrival without involving any further purification.

### 2.2. Fabrication process and characterization of the electrode array

The preparation of stretchable electrode array is as following. Firstly, a soft stretchable substrate was prepared using silicon rubber mixture (Ecoflex 0020) [39]. It was composed of part A and part B of Ecoflex in a mass ratio of 1:1. The mixed Ecoflex was evenly spun onto the acrylic plate with the speed to 200 r/min and then cured at 60 °C for 15 min. Secondly, gold particles were evaporated to the surface of Ecoflex using a thermal evaporation device, and a mask was employed to form the electrodes on Ecoflex. Next, the liquid metal was rolled to the appropriate position and the pin interface was wrapped with a small amount of liquid metal to connect with the flexible stretchable electrode array and then fixed with glue. The interface was encapsulated with Ecoflex. Finally, the stretchable electrode array was built and stored in room temperature for later use.

The tensile properties of the electrode array were tested by an AG-X Plus universal testing machine (Japan). The resistance variation trend of the electrode under different strains was obtained. Considering that tensile strain of skin surface caused by body movement typically will not exceeding 50 %, the electrode has undergone repeated single tensile test and cyclic tensile test under 50 % strain. Field-emission scanning electron microscopy (FESEM, Phenom Pharos) was used for studying the

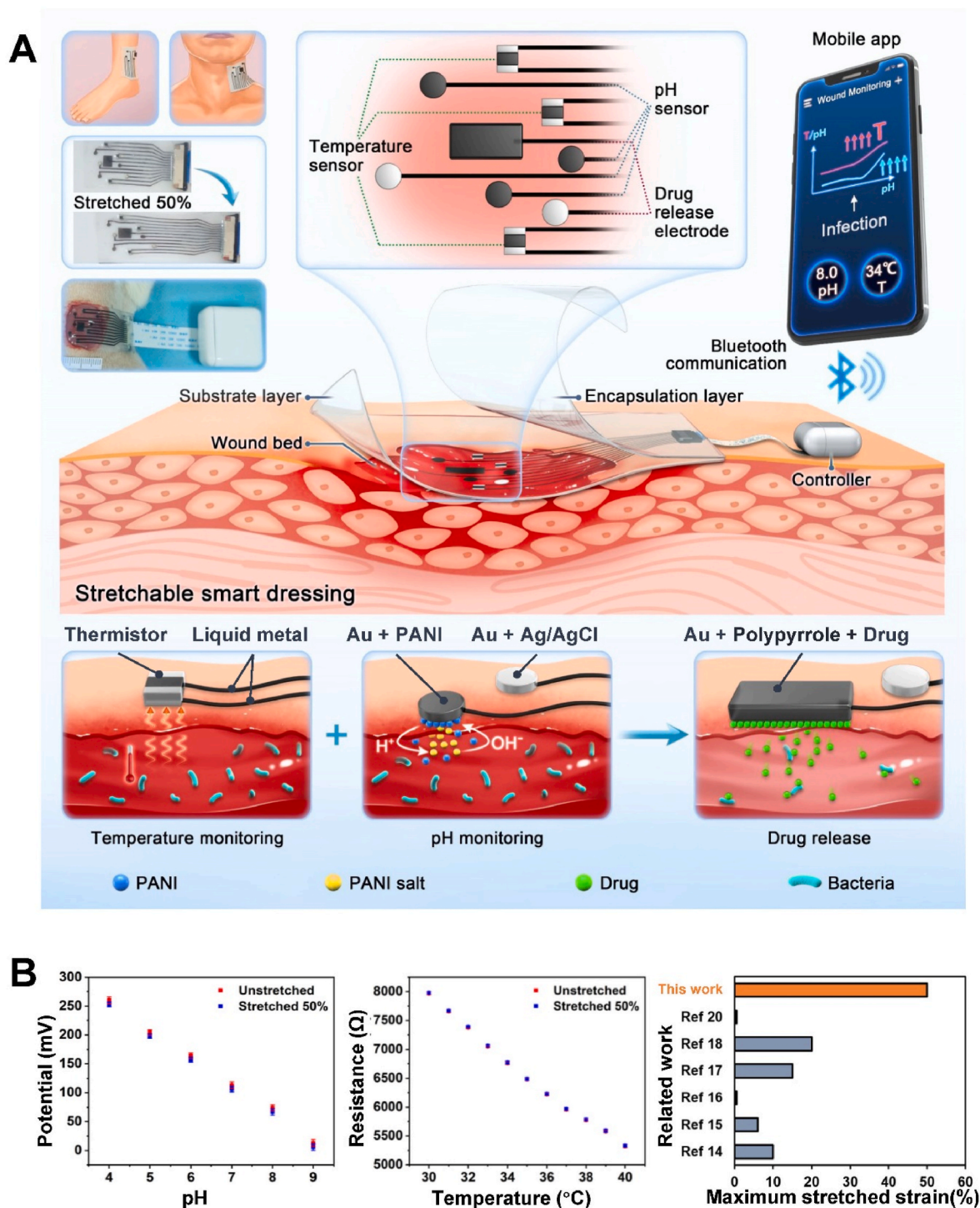


**Fig. 1.** Soft stretchable smart wound dressing for wound infection monitoring and treatment. (A) Schematic diagram of the smart dressing patched on the wound site for bacterial infection detection by simultaneous monitoring the changes of temperature and pH value, and providing treatment via electrically controlled drug releasing. (B) Stretchability of the smart dressing.

morphologies of the liquid metal, PANI, Au, and Ag/AgCl.

### 2.3. Fabrication and characterization of the pH sensor

The pH sensor was constructed with three working electrodes based on PANI and a reference electrode based on Ag/AgCl. The PANI was polymerized onto the working electrodes by cyclic voltammetry from  $-0.2$  V to  $1$  V versus. By dropping the Ag/AgCl ( $10 \mu\text{L}$  ink) onto the Au surface within a  $1$  mm radius area and further covering a layer of

polyvinyl butyral (PVB) containing KCl, a reference electrode was built. Finally, the pH sensor was formed after being dried at room temperature.

The performance test of the pH sensors included the following: (i) Sensitivity and repeatability of the pH sensors. The standard solution with pH value of  $4\sim 9$  was calibrated. The pH sensors were tested for  $60$  s for each pH value. (ii) Selectivity of the pH sensors. The prepared solution included  $10 \text{ mM Ca}^{2+}$ ,  $10 \text{ mM Na}^{+}$ ,  $10 \text{ mM K}^{+}$ , and  $10 \text{ mM Cl}^{-}$ . (iii) Response time test. In response time test, the solutions of different

pH value were prepared with NaOH. (iv) Stability test of the pH sensors. Standard buffer solution (pH = 7, 8) was used to test the stability of the pH sensors for about 10 h. (v) Performance test of pH sensors under strain. Using standard buffer solution (pH = 7, 8), the stretchable properties of the pH sensors was tested from 0 to 50 % strain.

#### 2.4. Fabrication and characterization of the temperature sensor

The temperature sensor was made of commercial thermistor 0805. The circuit of the designed temperature sensor was coated with a layer of liquid metal evenly, and the chip was placed in the corresponding position. Finally, it was encapsulated by Ecoflex.

The performance test of the temperature sensors included the following: (i) Sensitivity and repeatability of the temperature sensors. The temperature sensors were calibrated from 30 °C to 40 °C and tested for 600 s for each temperature value. (ii) Response time test. The temperature sensors were tested with temperature value ranging from 37 °C to 40 °C. (iii) Stability test of the temperature sensors. The stability of the temperature sensors was tested for about 12 h. (iv) Performance test of temperature sensors under strain. The stretchability of the temperature sensors was tested from 0 to 50 % strain.

#### 2.5. Fabrication and characterization of the drug electrode

The platinum counter electrode and Ag/AgCl reference electrode were deposited with PPy/cefazolin sodium film. First, by applying a constant current of 4 mA on the electrodes for 200 s in the mixed solution of 0.2 M pyrrole and 0.02 M cefazolin sodium, the PPy/cefazolin layer was formed. Then the drug electrode was rinsed with PBS solution. Finally, the as-prepared electrodes were stored in wet environment after being rinsed with DI water. The concentration of the drug was confirmed by the experimental screening, which was only applicable to this animal experimental model, and the early infection phenomenon was successfully monitored during wound monitoring, providing a signal for drug administration. Normal wound healing takes around 3 weeks, and even longer after infection.

Characterization of the drug electrodes: (i) Drug release test. The drug electrode was released into 2 mL PBS solution. Voltage stimulation was  $-0.5$  V each time for 30 s. The sample was analyzed by nanodrop. Based on the absorbance of a specific wavelength (272 nm), a calibration curve was obtained for measuring the concentration of the solution. For comparison, the concentration of drug by spontaneous release and electric stimulation release were measured respectively. (ii) Performance test of drug electrodes under strain. The stretchability of the drug electrodes was tested at 0–50 % strain.

#### 2.6. Antibacterial activity evaluation

First, 10 mL liquid broth (LB) culture medium was prepared and 100  $\mu$ L of a single colony of *S. aureus* was inoculated into it at 37 °C overnight. The 100  $\mu$ L of bacterial suspension was then spread onto agar plates in several 6-cm petri dishes, which were placed into incubator overnight. Three groups were prepared, each consisting of two Petri dishes. *S. aureus* in the control group did not need to be treated, and the buffer solution released by the drug electrode was added to the Petri dish in the experimental group. In the next day, the number of colonies was counted.

#### 2.7. In vitro biocompatibility assessment

Mouse L929 cells were used to study the biocompatibility of the smart dressing using CCK-8 assay. L929 cells were cultured in DMEM (Gibco) supplemented with 10 % FBS (Sigma) and 1 % penicillin/streptomycin (Cytiva) at 37 °C in a humidified atmosphere of 5 % CO<sub>2</sub>. All materials were soaked in fresh culture medium (3 cm<sup>2</sup> mL<sup>-1</sup>) and incubated in a humidified incubator (5 % CO<sub>2</sub>) at 37 °C for 24 h. The

cells were seeded in a 96-well plate at a density of  $1 \times 10^4$  cells per well and incubated for 24 h. The cells were then exposed to the different extracts for 24 h and cell viability was assessed using a CCK-8 kit (Beyotime) according to the manufacturer's instructions. Cells cultured with complete growth medium, extracts of HD-polyethylene were considered as blank and negative controls, respectively. Cell viability was calculated as relative percentage of living cells compared to the blank control.

#### 2.8. Wound infection monitoring

Using *S. aureus*, a rat model of wound infection was created for evaluation of wound infection detection. Female Sprague Dawley (SD) rats were supplied by Beijing Charles River Animal Co., Ltd. In the animal experiment, nine 6-week-old SD rats were used. All animal experiments conformed to the National Institutes of Health guidelines, and protocols were approved by the Institutional Animal Care and Use Committee (IACUC) of Shenzhen Institutes of Advanced Technology Chinese Academy of Sciences (SIAT-IACUC-20210311-YY5-TXXZX-ZXL-A1390-01).

The animals were divided into three groups: uninfected, infected, and post infection administration. To make a cutaneous wound on the back of the rats, the rats were anesthetized with isoflurane and the dorsal hair was shaved with the back skin being exposed. The shaved area was then sterilized with 75 % alcohol and iodine, after which a square full-thickness skin wound (2 cm  $\times$  2 cm) was created by using scissors. Using sterilized forceps and scissors respectively, the fascia part of the lower dermis was removed and the fascia was destroyed. Bacterial infection was induced by inoculating *S. aureus* suspension (50  $\mu$ L,  $1 \times 10^9$  CFU) to the wounds that have been washed with saline and blotted with sterile gauze. The wounds of the rats in the control group were processed with physiological saline. The smart dressings were attached to wound beds for wound conditions monitoring, after which transparent 3 M dressings were used to cover the whole wound sites. The pH and temperature were monitored at 0, 1, 2, and 3day. The wound tissue of rats was obtained at an appropriate time.

#### 2.9. Histologic analysis

At 6 and 30 h, a biopsy of the wounded tissue was performed. All samples were firstly fixed in neutral formalin (10 %) for 24 h. After that, all samples were washed in running water for 3 h and then dehydrated in a graded ethanol series. Finally, all the samples were embedded in paraffin. Sections (6  $\mu$ m thick) which cut from each paraffin block were placed on glass slides and examined under the light microscopy after being deparaffinized, rehydrated, stained with hematoxylin and eosin (H&E).

#### 2.10. Statistical analysis

Data are expressed as mean  $\pm$  standard deviation (S.D.). The statistical techniques employed for analysis were two-tailed Student's t-tests between two groups and one-way ANOVA between more than two groups. A statistical significance of  $p < 0.05$  was represented by asterisks (\*).

### 3. Results and discussion

#### 3.1. Stretchability test of soft electrode

The performance of a soft electrode is determined by its stretchability. Characterizing the effect of stretching deformation on the electrical property is significant. Under normal conditions, electrode stretching is usually accompanied by obvious resistance changes and most existing strain sensors were developed based on this principle. However, in the application scenario of wound monitoring, stable

electrical performance is an important guarantee for accurate monitoring. Fig. 2 shows the stretchability of this soft dressing.

The circuit of the dressing was mainly composed of two electrodes, the liquid metal/gold composite electrode and the liquid metal electrode, and the interface was also connected with the liquid metal. Surface of liquid metal is difficult to be electrochemically modified, the liquid metal-gold composite circuit is used in this work, and the conductive tensile ratio is mainly contributed by gold. Fig. 2A and B show the microscopic morphology of the two electrodes respectively. Through the process of hot evaporation, the gold spontaneously forms a fold morphology on the substrate, and this special morphology gives it stretchable properties. It can be seen on Fig. 2B, liquid metal has intrinsic stretchability and can be fully infiltrated with other metals. The microstructure did not change significantly, so the tensile conductivity was relatively stable. The resistance of the liquid metal/gold composite electrode changed gently with the strain. Within the strain range of 50 %, its resistance changed from 525  $\Omega$  to 550  $\Omega$  over 50 % strain range (Fig. 2C). Its resistance change rate was less than 0.06 (Fig. 2D), which indicated that the electrical performance of the electrode was quite stable under this strain. The resistance changes of the two electrodes under different stretching rates are shown in Fig. S2 and Fig. S3 respectively. It can be seen that the resistance change of liquid metal is approximately linear, which is related to its excellent conductivity.

Under different strains, its absolute resistance change is very small. The liquid metal-gold composite electrode maintains with constant resistance at the strain of 10 % and the resistance slowly increases with the strain reaching 20 %. When the strain range is between 20 % and 50 %, the rate of change in resistance is also close to linear. The property is associated with its morphology. The above results demonstrate the stable performance of sensors within 50 % strain. After 1000 cycles of testing, Fig. 2E shows that the electrical performance of the electrode did not change at all. The liquid metal electrode showed the same stable stretchability. Fig. 2F shows the relationship between resistance and strain during a single stretch of the liquid metal electrode. It can be seen that at 50 % strain, the resistance variation range was less than 1  $\Omega$  (Fig. 2F) and the resistance variation rate was also low, within 0.14. The loop test again proved its stability. Liquid metal has low resistance and good tensile conductivity. However, its surface tension is large, and as a fluid, it cannot be electrochemically modified on the surface, which limits its application in the field of sensors. Therefore, we choose to modify the gold electrode to obtain different sensors, and the liquid metal is used in the composite circuit to improve the electrical conductivity. The minimal resistance change did not affect the temperature sensor based on the temperature-sensitive resistor. Although the resistance of the two conductive lines changes at 50 % strain, the amount of change is relatively small, and this small change will not have a significant impact on

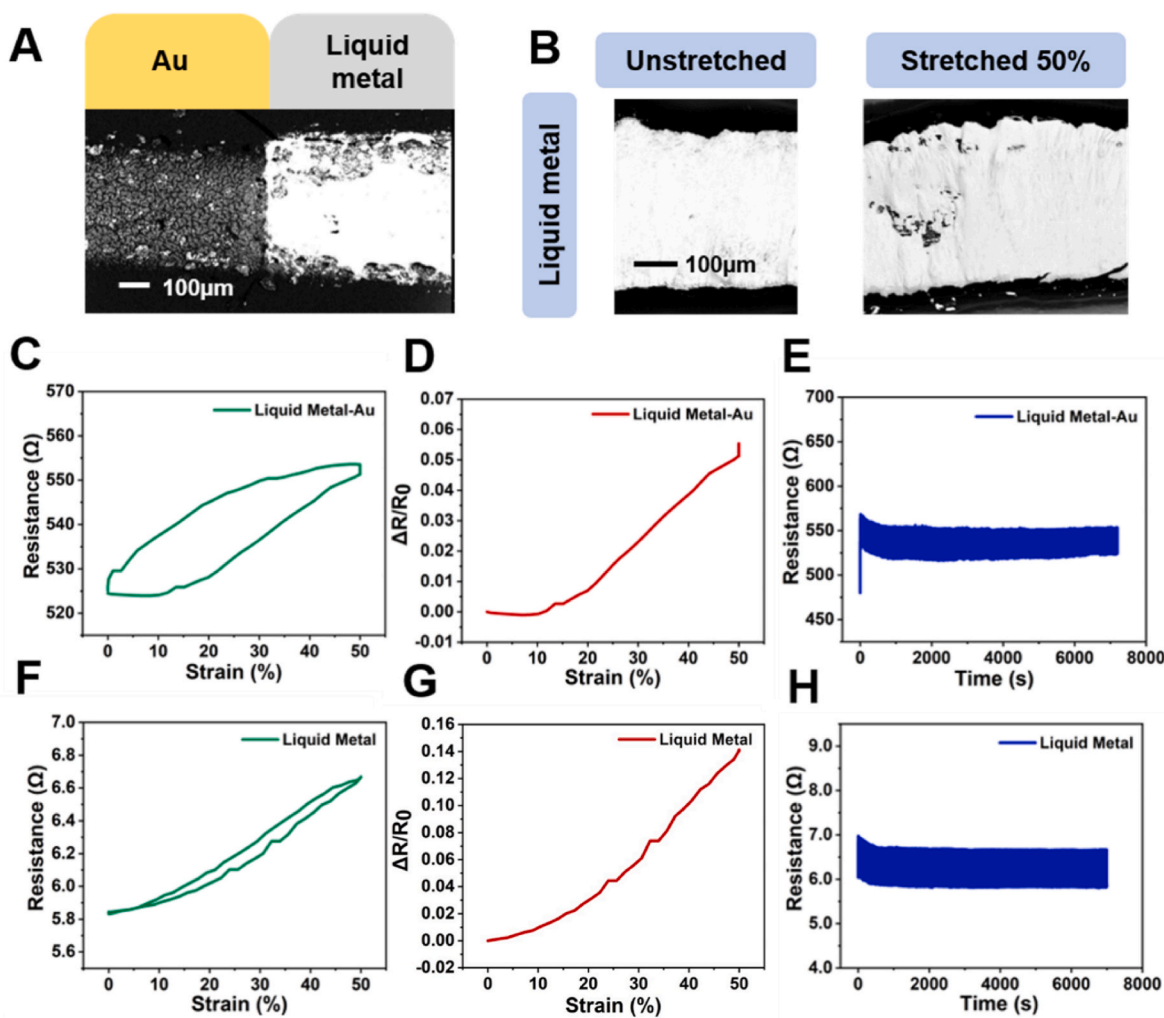


Fig. 2. Stretchability test of soft electrode. (A) SEM graphics of liquid metal/gold composite electrode. (B) SEM graphics of the liquid metal electrode. (C) Single tensile test of liquid metal/gold electrode. (D) The resistance rate of the liquid metal/gold electrode under tensile strain. (E) Cyclic tensile test of liquid metal/gold electrode. (F) Single tensile test of liquid metal electrode. (G) The resistance rate of the liquid metal electrode under tensile strain. (H) Cyclic tensile test of liquid metal electrode. (For interpretation of the references to color in this figure legend, the reader is referred to the Web version of this article.)

its performance. It can be seen from Fig. S1 that the deformation exceeds 300 % and the stress is less 0.1 N, indicating that its elastic modulus is low and the material is very soft.

Usually, the deformation of human skin is less than 50 %, and the mean failure strain of human skin was  $54 \% \pm 17 \%$  as reported [40]. Therefore, most stretchable sensor for skin was investigated with the strain up to 50 % [41]. Fig. 2C and F show that the resistance change rate of the circuit is low when the strain change is 50 %. Therefore, the dressing can maintain relatively stable performance within a strain range of 50 %. Usually, the change of morphology and structure affects the properties of the electrode. The dressing is composed of the above two circuits, and the data show that both circuits have good electrical conductivity and tensile stability. But the morphology of the stretchable electrode based on liquid metal was almost unchanged during the drawing process, so its electrical property was relatively stable during the drawing process. A variety of sensors were integrated on electrodes to achieve stretchability of the sensor.

### 3.2. Performance characterization of the temperature sensor

With the advancement of electronic technology, more and more miniature resistors have been commercialized. The 0805 type chip resistor has a small package volume, good temperature response,

which was used as a temperature sensor for the smart dressing by connecting with liquid metal. The resistance of negative temperature coefficient materials decreases as the temperature rises. Commercial thermistors based on this principle have good accuracy and can be used as temperature sensors. Fig. 3A shows the actual temperature sensitive resistor. Its volume is only  $0.8 \times 1.2 \times 1.6$  mm, which fully fit with the liquid metal electrode. By infiltrating a little liquid metal at both ends of the temperature sensor, the temperature sensor was reliably combined with the liquid metal circuit. The external encapsulation layer was also made to ensure the reliability of the overall structure and no slippage in resistor position.

Liquid metal had little effect on the resistance change of the thermistor because of low enough resistivity, thus the accuracy of the temperature sensor was guaranteed. Commercial temperature sensor chips have different resistance values at different temperatures. When it was integrated on the Ecoflex substrate, its resistance changed due to the thermal conductivity of the substrate. Firstly, the resistance of the temperature sensor within 30–40 °C was calibrated. As can be seen from Fig. 3B, different temperatures had corresponding relatively stable resistances, and the jagged change was caused by the temperature fluctuation of the heating table. The result showed that the temperature and the resistance were linearly related (Fig. 3C). By linear fitting, the relationship between the temperature and the resistance could be

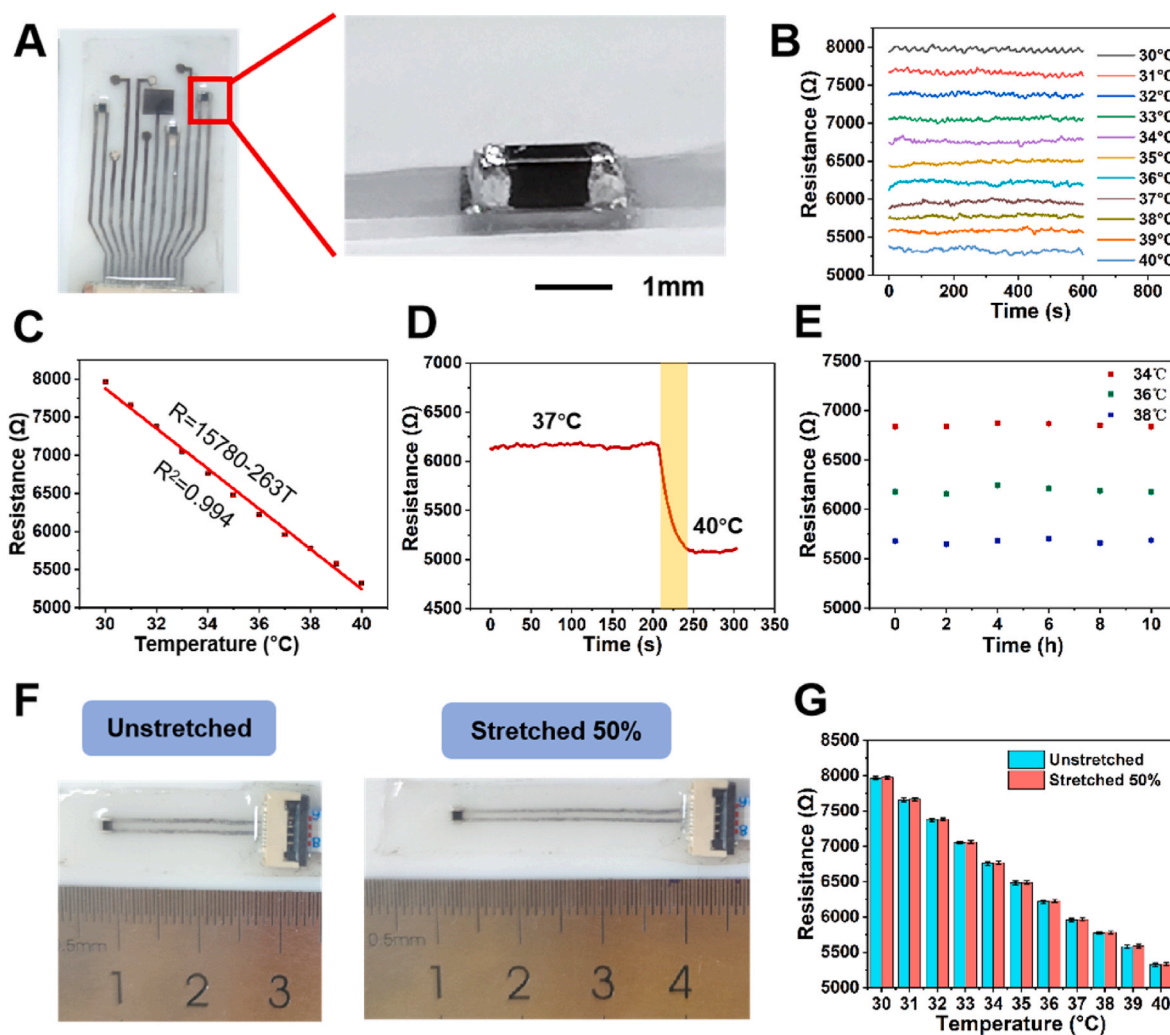


**Fig. 3.** Performance characterization of the temperature sensor. (A) The physical diagram of the circuit connection of the temperature sensor. (B) The resistance calibration of the temperature sensor in the range of 30 °C–40 °C. (C) The linear fitting of the resistance of the temperature sensor in the range of 30 °C–40 °C. (D) The response time of the temperature sensor. (E) Stability test of temperature sensor within 10 h. (F) Photos of the stretched temperature sensor. (G) Resistance characteristic of temperature sensor under stretching.

calibrated. The response time of the temperature sensor is shown in Fig. 3D. It can be seen from the experimental data that when the temperature increased, the resistance decreased rapidly and reached a relatively stable trend within 30s. During the temperature maintenance process, the heating table is adjusted with the real-time temperature change, which makes it impossible to keep the temperature at a certain value very accurately. The temperature sensor exhibited good stability through long-term intermittent testing (Fig. 3E). The temperature sensor fabricated based on the soft electrode had good stretchability (Fig. 3F). It can be seen from Fig. 3G that the resistance change of the sensor was negligible under 50 % strain, which indicated that the sensor could

maintain normal working while being fully stretched.

### 3.3. Performance characterization of the pH sensor

A standard pH sensor usually consists of a working electrode and a reference electrode. The principle of the pH sensing is based on the measurement of electrical potential difference between the two electrodes, which is produced by the protonation reaction of polyaniline (PANI). In this smart dressing, three working electrodes correspond to one reference electrode. It can be seen from Fig. 4A that the PANI on the working electrode was discretely distributed, which indicated that its

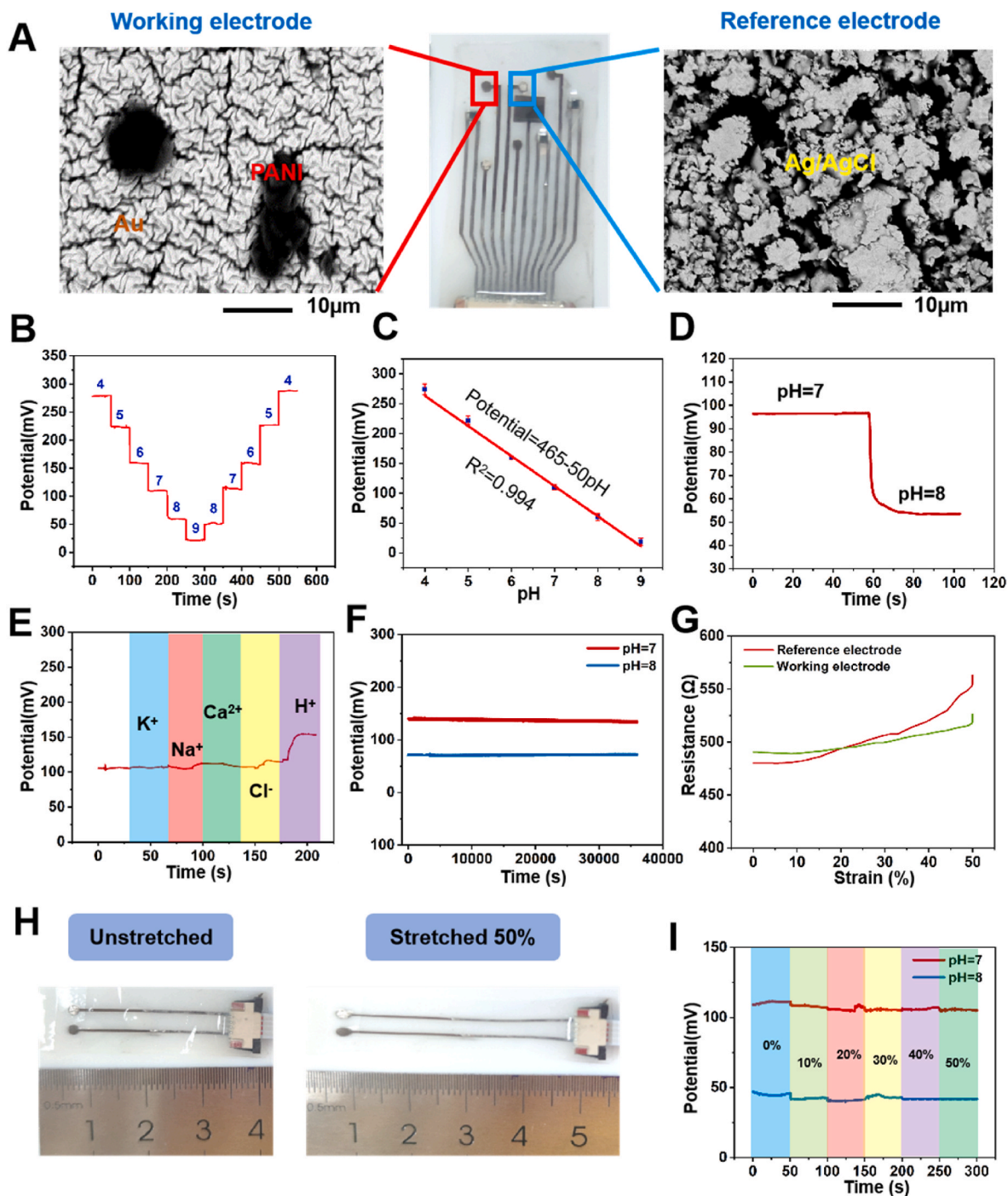


Fig. 4. Performance characterization of the pH sensor. (A) Physical and microscopic morphology of pH sensor. (B) Calibration of pH sensor. (C) Potential linear fitting of pH sensor. (D) Response time of pH sensor. (E) Specific detection of pH sensor. (F) Stability test of pH sensor. (G) Resistance characteristic of pH sensor under tensile deformation. (H) Photos of stretched pH sensor. (I) Potential test of pH sensor in stretched state.

morphology would hardly be affected by strain. The reference electrode was composed of Ag/AgCl, which appeared as some accumulated debris in the SEM image. The microscopic morphology of the two electrodes contributed to the stretchability of the sensor.

In the performance test, the pH sensor was first calibrated. As shown in Fig. 4B, the sensor showed a good step change with the pH scale ranging from 4 to 9. Fig. 4C shows that the formula of the potential with respect to pH could be obtained by linear fitting, exhibiting good linear behavior ( $r^2 = 0.994$ ). The pH sensor needed a fast response time. With the pH value changing from 7 to 8, the pH sensor completed the potential transition within 20s, which indicated that the response speed of the sensor was rapid (Fig. 4D). Human tissue fluid contains a variety of ions, thus the specificity of the sensor needs to be verified. In the same solution, with the addition of different ions such as  $K^+$ ,  $Na^+$ , and  $Ca^{2+}$ , the potential maintained steady with small fluctuation, which was caused by the sudden change of the solution concentration. When hydrogen ions were added, the sensor exhibited a specific response and the potential plateau changed rapidly, indicating that the sensor had good specificity (Fig. 4E). The unique protonation reaction of polyaniline, when the hydrogen ion concentration increases, polyaniline will get positive charge, self-potential increases, and vice versa. Fig. 4F shows that the pH sensor could maintain a relatively stable potential plateau through continuous testing for up to 10 h. The shift in potential

occurred during the test was less than 2mv/h, which indicated that the change in pH was only 0.04 per hour. Overall, the pH sensor exhibited superior stability.

In practical applications, the sensor will face deformation caused by stretching, thus the stretchability of the sensor needs to be confirmed. During the stretching process, it can be seen in Fig. 4G that the resistances of both the working electrode and the reference electrode slightly changed. Fig. 4H shows a physical image of the sensor stretching and the pH test during stretching can be seen in Fig. 4I. As the strain increased, the potential plateau of the sensor underwent small fluctuations at the moment the strain changed. When the strain reached 50 %, the potential drifted by about 10mv, and the error of pH was less than 0.2, which was small enough to allow the sensor to maintain good performance during stretching. The pH sensor obtained by electrochemical modification had good performance and could maintain relatively accurate monitoring at 50 % strain.

### 3.4. Characterization of drug electrodes

The drug electrode consisted of a reference electrode and a working electrode. The reference electrode was the same as the pH sensor, which was composed of Ag/AgCl. The working electrode for drug loading and releasing was based on polypyrrole (PPy). The drug is Cefazolin

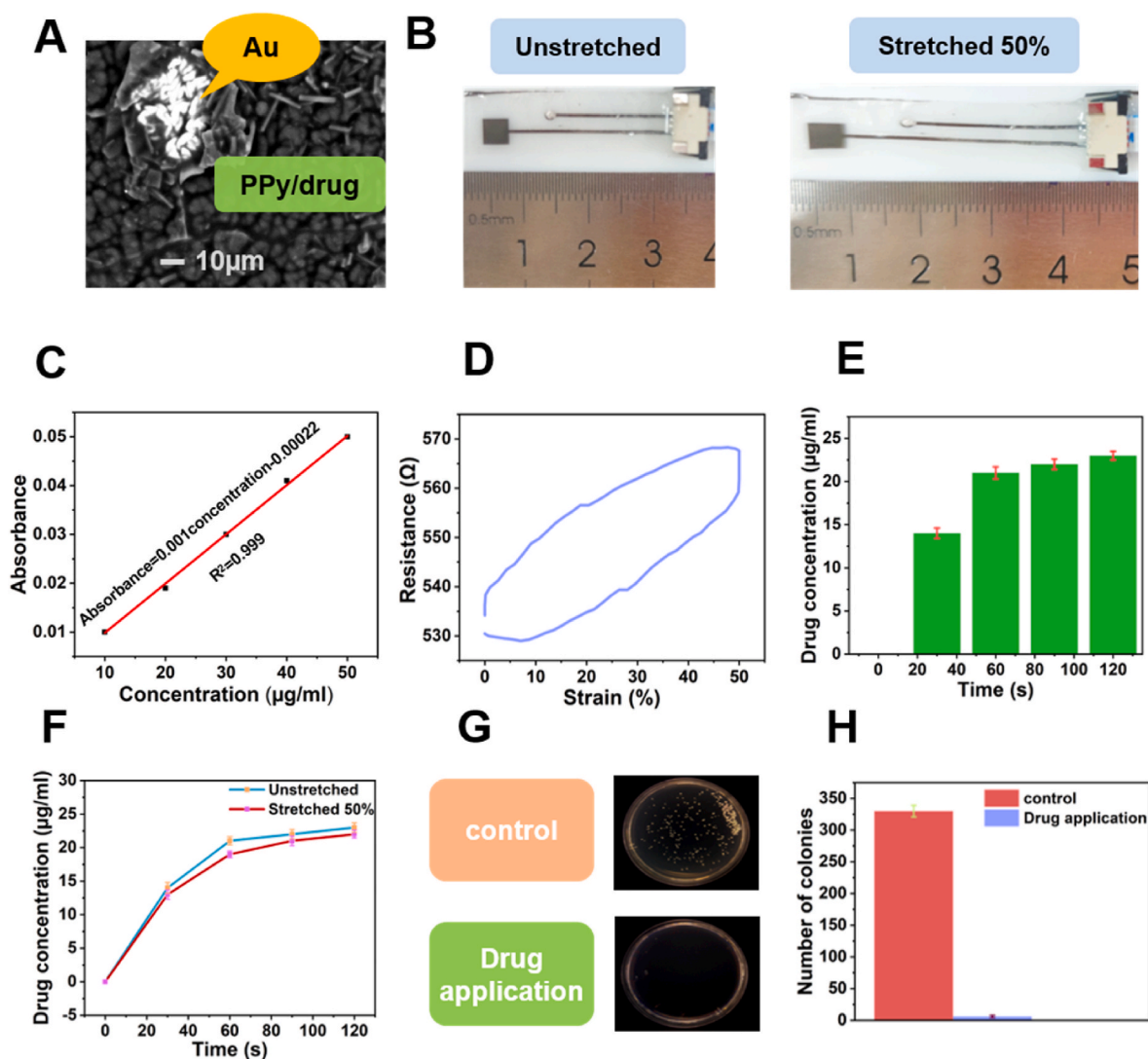


Fig. 5. Characterization of drug electrodes. (A) SEM image of the drug electrode. (B) Photos of the stretched drug electrode. (C) Drug release calibration. (D) Stretching test of the drug electrode. (E) Drug release test. (F) Stretchability test of the drug electrode. (G) Antibacterial test diagram. (H) Bacterial colony statistics.

sodium, a common antibiotic. PPy based drug loading and releasing is a promising method. The principle is anodized polymerization of drug, which can be controlled by voltage. The optimal release rate can be obtained by selecting the appropriate voltage based on the previous research. With voltage stimulation, the drug released faster than nature release from PPy [20,42]. Fig. 5A shows the microscopic morphology of the drug electrode. It can be seen that the polypyrrole layer with the drug cefazolin sodium covered the electrode. The calibration of drug concentration can be seen from Fig. 5C. Within a certain concentration range, there was a good linear correlation between drug concentration and absorbance. Compared with drug release under voltage stimulation, the electrode will also release the drug without applying voltage as shown in Fig. S4. As the drugs are carried by the electrode based on charge and discharge operation, a portion of the drugs will leak over time. But the electrode with applied voltage has a significantly faster drug release rate, indicating that electrically controlled drug application

can be achieved.

In addition, the drug electrode could also achieve stretchability. After tensile test, the electrical property of the electrode after PPy modification was not greatly affected. Under 50 % strain, the resistance changed within 40  $\Omega$  and the resistance change rate was less than 0.08 (Fig. 5D). Drug release behavior under electrical stimulation was showed on Fig. 5E. It can be seen that the drug release rate exceeded 80 % in around 60s. When the dressing is stretched, the drug-carrying electrode also needs to maintain a relatively stable drug release capacity. Fig. 5F shows that 50 % strain did not have a significant effect on drug release. The drug electrode had good stretchability and could release the drug in a short time when stimulated by electricity.

The antibacterial performance of the drug was verified. Fig. 5G shows the antibacterial experiment of the drug. It can be clearly seen that, compared with the control group, almost no colonies survived in the medium treated with the drug, which was also verified by the colony

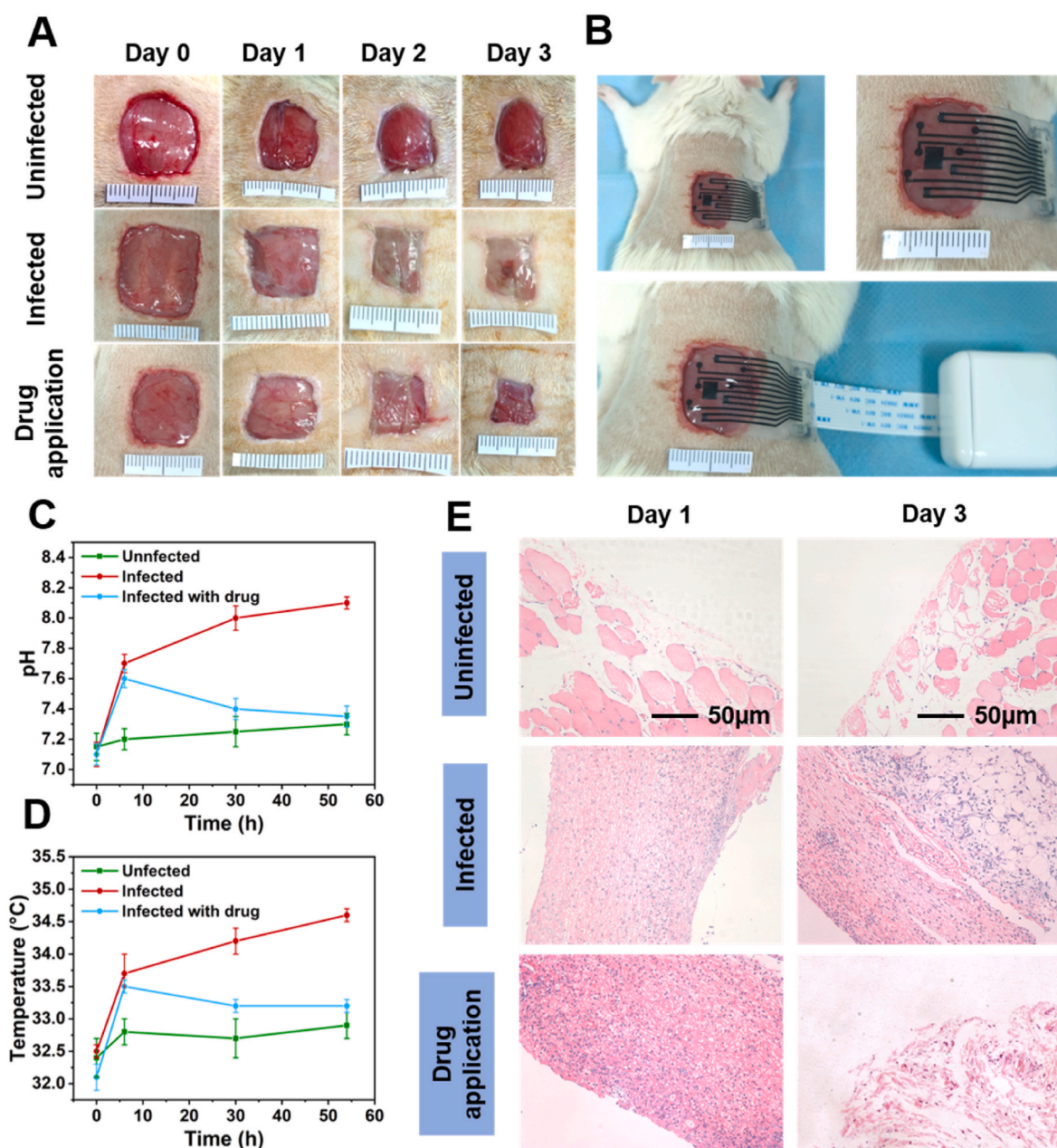


Fig. 6. Validation of animal models. (A) Rat wounds in different groups over 4 days. (B) Rat wound monitoring using the smart dressing. (C) pH monitoring of wounds. (D) Temperature monitoring of wounds. (E) Tissue section of wounds.

statistics in Fig. 5H, indicating that the drug had good resistance to *Staphylococcus aureus*.

### 3.5. Wound infection monitoring and treatment

In order to verify the actual role of the smart dressing in wound monitoring, a local infection model in rats was constructed. For the wounds of rats, three treatments were performed. Fig. 6A shows the three types of wounds at 0–3 days. After 3 days, the wound tissue fluid decreased and effective data could not be obtained. The control group was a blank control and the wound was not treated. It can be seen that the wound gradually shrunk over time, and there was no obvious trace of infection during the process. The experimental group was divided into two categories with one as artificial inoculum. *Staphylococcus aureus* was inoculated into the wound site. As shown in Fig. 6A, the wound had a pus-like discharge and a covering had formed, which was a typical symptom of bacterial infection. When another type of treatment was administered to wounds after infection, the wound state with the drug applied became significantly better and the recovery trend was also faster. It can be seen from the wound status that the wound of the administered rats recovered quickly, and the infected rats showed obvious signs of suppuration. These types of wounds were monitored separately. As can be seen from Fig. S6, the wound healing rate after drug treatment was higher than that of the other two groups. Infected wounds have the lowest rate of healing, because the infection causes the wound to remain in the inflammatory stage, extending the healing time. Fig. 6B shows the application state of the dressing on the back of the rat. The soft enough substrate was very common with the skin of the rat's back. The external Bluetooth module could obtain the data in real time. The infection causes persistent inflammation, which can lead to the wound healing failure. After the drug controls the inflammatory environment, the transition from the inflammatory period to the tissue healing period can be achieved.

The pH data of the wound is shown in Fig. 6C. It can be seen that the pH of the normal wound increased slightly over time, which was due to the presence of plasma in the wound, resulting in a neutral pH value. The pH of infected wound surface increased significantly at the 6th hour due to the physiological changes caused by bacterial infection and keep increasing with the aggravation of infection. As for the infected wounds treated with drug administration, the pH of the wound increased at the early stage of infection while it kept decreasing in the subsequent period but not yet reaching back to the normal level. Fig. 6D shows the temperature change of the wound surface. The temperature of the normal wound tended to be relatively stable, fluctuating at 32.5 °C. However, the temperature of the infected wound increased significantly, rising from 32.5 °C to 33.7 °C, which was due to the inflammatory reaction caused by bacterial infection. The wound temperature after administration also showed a downward trend, but it was still slightly higher than that of normal wounds, presumably due to insufficient drug dosage. The drug release behavior *in vivo* is influenced by many factors and may be different from *in vitro* results, which is deserved further research. It can be seen from Fig. 6C and D, the wounds of the experimental group of rats were monitored after administration. After early infection, there was a clear trend of improvement in the wound area, indicating that the drug had an effect on the infection.

Tissue sections at different times were observed as shown in Fig. 6E. It can be seen that the wound sections of the three different treatments were very different. At different time periods, only a small amount of inflammatory factors were observed in normal wound slices and more normal muscle cells were observed. A large number of inflammatory factors could be observed in the infected tissue slices on the first day. Over time, the distribution of inflammatory factors became more dense and the tissue presented a state of edema. Inflammatory factors were also dense in infected wounds before administration, but were significantly improved after administration. The experimental results showed that inflammatory factors were significantly reduced in wound tissue

sections of rats in the experimental group, which confirmed that the drug release had an inhibitory effect on infection. Overall, by monitoring chemical signals, changes in pH and temperature can be detected within 6 h of infection occurring, providing theoretical possibilities for rapid diagnosis and treatment of early infection.

Good biocompatibility is essential for the materials used in a wound dressing to ensure that the dressing will not cause damage to the wound bed when in contact with the wound surface, which was studied by the viability of L929 cells exposed to the material extracts. The results showed that all of these substrates did not induce significant cytotoxicity including Ecoflex, Ecoflex contained liquid metal, and the final smart dressing, as the relative cell viability was greater than 95 % (Fig. S5). These results confirmed that smart dressing is biocompatible.

The above results showed that the smart dressing successfully monitored the changes of physiological parameters caused by wound infection. Clinically, the prevention and treatment of early infection could greatly reduce the suffering of patients. Changes in pH and temperature caused by wound infection were observed at 6 h and this method had better timeliness than conventional clinical methods. In addition to accurate monitoring function, wound dressings also need suitable breathability and their performance will be continuously improved with material optimization. The pus from infected wounds would affect the sensor's monitoring of wound pH and temperature. This smart dressing could benefit the severe wound treatment in clinic when the wound is not able to observe directly, such as vacuum sealing drainage (VSD) therapy. Timely detection of infection can avoid delayed healing caused by infection.

## 4. Conclusion

The study produced a stretchable smart dressing for wound monitoring and healing. The substrate of the smart dressing had a modulus close to that of the skin, which made it comfortable to wear. Through the introduction of liquid metal electrodes, the device had full-layer stretchability and the stability of the soft and hard interface was also guaranteed. Various stretchable sensors integrated on the electrodes exhibited good performance. Through a series of *in vitro* tests and animal model validation, it was confirmed that the dressing could monitor changes in pH and temperature caused by wound infection in rats. It acted as a sentinel for the monitoring of early clinical infection.

### CRedit authorship contribution statement

**Rui Su:** Writing – original draft, Methodology, Investigation. **Liang Wang:** Writing – original draft, Visualization, Validation, Investigation. **Fei Han:** Writing – review & editing. **Shaoquan Bian:** Writing – review & editing. **Fengzhen Meng:** Writing – review & editing, Investigation. **Weichen Qi:** Writing – review & editing, Methodology. **Xinyun Zhai:** Writing – review & editing. **Hanfei Li:** Writing – review & editing, Methodology. **Jun Wu:** Writing – review & editing. **Xiaohua Pan:** Writing – review & editing. **Haobo Pan:** Writing – review & editing. **Peizhi Guo:** Writing – review & editing. **William W. Lu:** Writing – review & editing. **Zhiyuan Liu:** Writing – review & editing, Supervision, Project administration, Conceptualization. **Xiaoli Zhao:** Writing – review & editing, Supervision, Project administration, Conceptualization.

### Declaration of competing interest

The authors declare that they have no known competing financial interests or personal relationships that could have appeared to influence the work reported in this paper.

### Data availability

Data will be made available on request.

## Acknowledgements

This work was supported by the National Key R&D Program of China (grant no. 2022YFC2403000), National Natural Science Foundation of China (grant no. 32201125), Guangdong Basic and Applied Basic Research Foundation (grant no. 2021A1515110902), Science and Technology Research Funding of Shenzhen (grant no. JCYJ20200109150420892, KQTD20210811090217009).

## Appendix A. Supplementary data

Supplementary data to this article can be found online at <https://doi.org/10.1016/j.mtbio.2024.101107>.

## References

- [1] S.A. Eming, P. Martin, M. Tomic-Canic, Wound repair and regeneration: mechanisms, signaling, and translation, *Sci. Transl. Med.* 6 (2014) 265sr266, <https://doi.org/10.1126/scitranslmed.300933>, 265sr266.
- [2] G.C. Gurtner, S. Werner, Y. Barrandon, M.T. Longaker, Wound repair and regeneration, *Nature* 453 (2008) 314–321, <https://doi.org/10.1038/nature07039>.
- [3] M.A. Fonder, G.S. Lazarus, D.A. Cowan, B. Aronson-Cook, A.R. Kohli, A. J. Mamelak, Treating the chronic wound: a practical approach to the care of nonhealing wounds and wound care dressings, *J. Am. Acad. Dermatol.* 58 (2008) 185–206, <https://doi.org/10.1016/j.jaad.2007.08.048>.
- [4] G. Han, R. Ceilley, Chronic wound healing: a review of current management and treatments, *Adv. Ther.* 34 (2017) 599–610, <https://doi.org/10.1007/s12325-017-0478-y>.
- [5] M.S. Brown, B. Ashley, A. Koh, Wearable technology for chronic wound monitoring: current dressings, advancements, and future prospects, *Front. Bioeng. Biotechnol.* 6 (2018) 1–21, <https://doi.org/10.3389/fbioe.2018.00047>.
- [6] M. Abrigo, S.L. McArthur, P. Kingshott, Electrospun nanofibers as dressings for chronic wound care: advances, challenges, and future prospects, *Macromol. Biosci.* 14 (2014) 772–792, <https://doi.org/10.1002/mabi.201300561>.
- [7] V. Andreu, G. Mendoza, M. Arruebo, S. Irueta, Smart dressings based on nanostructured fibers containing natural origin antimicrobial, anti-inflammatory, and regenerative compounds, *Materials* 8 (2015) 5154–5193, <https://doi.org/10.3390/ma8085154>.
- [8] M. Parahani, A. Shafiee, Wound healing: from passive to smart dressings, *Adv. Healthcare Mater.* 10 (2021) 2100477, <https://doi.org/10.1002/adhm.202100477>.
- [9] W. Gao, C. Yu, Wearable and implantable devices for healthcare, *Adv. Healthcare Mater.* 10 (2021) 2101548, <https://doi.org/10.1002/adhm.202101548>.
- [10] S.H. Lu, M. Samandari, C. Li, H. Li, D. Song, Y. Zhang, A. Tamayol, X. Wang, Multimodal sensing and therapeutic systems for wound healing and management: a review, *Sens. Actuators Rep.* 4 (2022) 100075, <https://doi.org/10.1016/j.snr.2022.100075>.
- [11] S. Patel, F. Ershad, M. Zhao, R.R. Isseroff, B. Duan, Y. Zhou, Y. Wang, C. Yu, Wearable electronics for skin wound monitoring and healing, *Soft Sci.* 2 (2022) 9, <https://doi.org/10.20517/ss.2022.13>.
- [12] J. Kim, A.S. Campbell, B.E.-F. de Ávila, J. Wang, Wearable biosensors for healthcare monitoring, *Nat. Biotechnol.* 37 (2019) 389–406, <https://doi.org/10.1038/s41587-019-0045-y>.
- [13] C. Wang, E. Shirzaei Sani, W. Gao, Wearable bioelectronics for chronic wound management, *Adv. Funct. Mater.* 32 (2022) 2111022, <https://doi.org/10.1002/adfm.202111022>.
- [14] S.E. Gardner, R.A. Frantz, B.N. Doebbeling, The validity of the clinical signs and symptoms used to identify localized chronic wound infection, *Wound Repair Regen.* 9 (2001) 178–186, <https://doi.org/10.1046/j.1524-475x.2001.00178.x>.
- [15] M. Fierheller, R.G. Sibbald, A clinical investigation into the relationship between increased periwound skin temperature and local wound infection in patients with chronic leg ulcers, *Adv. Skin Wound Care* 23 (2010) 369–379, <https://doi.org/10.1097/01.ASW.0000383197.28192.98>.
- [16] D. Lou, Q. Pang, X. Pei, S. Dong, S. Li, W.-q. Tan, L. Ma, Flexible wound healing system for pro-regeneration, temperature monitoring and infection early warning, *Biosens. Bioelectron.* 162 (2020) 112275, <https://doi.org/10.1016/j.bios.2020.112275>.
- [17] Q. Pang, D. Lou, S. Li, G. Wang, B. Qiao, S. Dong, L. Ma, C. Gao, Z. Wu, Smart flexible electronics-integrated wound dressing for real-time monitoring and on-demand treatment of infected wounds, *Adv. Sci.* 7 (2020) 1902673, <https://doi.org/10.1002/advs.201902673>.
- [18] Y. Jiang, A.A. Trotsyuk, S. Niu, D. Henn, K. Chen, C.-C. Shih, M.R. Larson, A. M. Mermin-Bunnell, S. Mittal, J.-C. Lai, A. Saberi, E. Beard, S. Jing, D. Zhong, S. R. Steele, K. Sun, T. Jain, E. Zhao, C.R. Neimeth, W.G. Viana, J. Tang, D. Sivaraj, J. Padmanabhan, M. Rodrigues, D.P. Perrault, A. Chattopadhyay, Z.N. Maan, M. C. Leolou, C.A. Bonham, S.H. Kwon, H.C. Kussie, K.S. Fischer, G. Gurusankar, K. Liang, K. Zhang, R. Nag, M.P. Snyder, M. Janusz, G.C. Gurtner, Z. Bao, Wireless, closed-loop, smart bandage with integrated sensors and stimulators for advanced wound care and accelerated healing, *Nat. Biotechnol.* 41 (2023) 652–662, <https://doi.org/10.1038/s41587-022-01528-3>.
- [19] E. Shirzaei Sani, C. Xu, C. Wang, Y. Song, J. Min, J. Tu, S.A. Solomon, J. Li, J. L. Banks, D.G. Armstrong, W. Gao, A stretchable wireless wearable bioelectronic system for multiplexed monitoring and combination treatment of infected chronic wounds, *Sci. Adv.* 9 (2023) eadf7388, <https://doi.org/10.1126/sciadv.adf7388>.
- [20] G. Xu, Y. Lu, C. Cheng, X. Li, J. Xu, Z. Liu, J. Liu, G. Liu, Z. Shi, Z. Chen, F. Zhang, Y. Jia, D. Xu, W. Yuan, Z. Cui, S.S. Low, Q. Liu, Battery-free and wireless smart wound dressing for wound infection monitoring and electrically controlled on-demand drug delivery, *Adv. Funct. Mater.* 31 (2021) 2100852, <https://doi.org/10.1002/adfm.202100852>.
- [21] K. Youssef, A. Ullah, P. Rezaei, A. Hasan, A. Amirfazli, Recent advances in biosensors for real time monitoring of pH, temperature, and oxygen in chronic wounds, *Mater. Today Bio.* 22 (2023) 100764, <https://doi.org/10.1016/j.mtbio.2023.100764>.
- [22] Z. Liu, J. Liu, T. Sun, D. Zeng, C. Yang, H. Wang, C. Yang, J. Guo, Q. Wu, H.J. Chen, X. Xie, Integrated multiplex sensing bandage for in situ monitoring of early infected wounds, *ACS Sens.* 6 (2021) 3112–3124, <https://doi.org/10.1021/acssensors.1c01279>.
- [23] Z. Zhang, R. Su, F. Han, Z. Zheng, Y. Liu, X. Zhou, Q. Li, X. Zhai, J. Wu, X. Pan, H. Pan, P. Guo, Z. Li, Z. Liu, X. Zhao, A soft intelligent dressing with pH and temperature sensors for early detection of wound infection, *RSC Adv.* 12 (2022) 3243–3252, <https://doi.org/10.1039/D1RA08375A>.
- [24] Y. Gao, D.T. Nguyen, T. Yeo, S.B. Lim, W.X. Tan, L.E. Madden, L. Jin, J.Y.K. Long, F.A.B. Aloweni, Y.J.A. Liew, M.L.L. Tan, S.Y. Ang, S.D. Maniya, I. Abdelwahab, K. P. Loh, C.H. Chen, D.L. Becker, D. Leavesley, J.S. Ho, C.T. Lim, A flexible multiplexed immunosensor for point-of-care in situ wound monitoring, *Sci. Adv.* 7 (2021) eabg9614, <https://doi.org/10.1126/sciadv.abg9614>.
- [25] Y. Ling, T. An, L.W. Yap, B. Zhu, S. Gong, W. Cheng, Disruptive, soft, wearable sensors, *Adv. Mater.* 32 (2020) e1904664, <https://doi.org/10.1002/adma.201904664>.
- [26] S. Gong, Y. Lu, J. Yin, A. Levin, W. Cheng, Materials-driven soft wearable bioelectronics for connected healthcare, *Chem. Rev.* 124 (2024) 455–553, <https://doi.org/10.1021/acs.chemrev.3c00502>.
- [27] R. Maiti, L.C. Gerhardt, Z.S. Lee, R.A. Byers, D. Woods, J.A. Sanz-Herrera, S. E. Franklin, R. Lewis, S.J. Matcher, M.J. Carré, In vivo measurement of skin surface strain and sub-surface layer deformation induced by natural tissue stretching, *J. Mech. Behav. Biomed. Mater.* 62 (2016) 556–569, <https://doi.org/10.1016/j.jmbbm.2016.05.035>.
- [28] M. Ottenio, D. Tran, A. Ní Annaidh, M.D. Gilchrist, K. Bruyère, Strain rate and anisotropy effects on the tensile failure characteristics of human skin, *J. Mech. Behav. Biomed. Mater.* 41 (2015) 241–250, <https://doi.org/10.1016/j.jmbbm.2014.10.006>.
- [29] T. Zhu, Y. Ni, G.M. Biesold, Y. Cheng, M. Ge, H. Li, J. Huang, Z. Lin, Y. Lai, Recent advances in conductive hydrogels: classifications, properties, and applications, *Chem. Soc. Rev.* 52 (2023) 473–509, <https://doi.org/10.1039/d2cs00173j>.
- [30] Y. Sun, W.M. Choi, H. Jiang, Y.Y. Huang, J.A. Rogers, Controlled buckling of semiconductor nanoribbons for stretchable electronics, *Nat. Nanotechnol.* 1 (2006) 201–207, <https://doi.org/10.1038/nnano.2006.131>.
- [31] D. Wan, J. Yang, X. Cui, N. Ma, Z. Wang, Y. Li, P. Li, Y. Zhang, Z.H. Lin, S. Sang, H. Zhang, Human body-based self-powered wearable electronics for promoting wound healing driven by biomechanical motions, *Nano Energy* 89 (2021) 106465, <https://doi.org/10.1016/j.nanoen.2021.106465>.
- [32] M. Sharifuzzaman, A. Chhetry, M.A. Zahed, S.H. Yoon, C.I. Park, S. Zhang, B. S. Chandra, S. Sharma, H. Yoon, J.Y. Park, Smart bandage with integrated multifunctional sensors based on MXene-functionalized porous graphene scaffold for chronic wound care management, *Biosens. Bioelectron.* 169 (2020) 112637, <https://doi.org/10.1016/j.bios.2020.112637>.
- [33] J. Li, X. Huang, Y. Yang, J. Zhou, K. Yao, J. Li, Y. Zhou, M. Li, T.H. Wong, X. Yu, Wearable and battery-free wound dressing system for wireless and early sepsis diagnosis, *Biorg. Transl. Med.* 8 (2023) e10445, <https://doi.org/10.1002/btm2.210445>.
- [34] X. Lin, Y. Mao, P. Li, Y. Bai, T. Chen, K. Wu, D. Chen, H. Yang, L. Yang, Ultra-conformable ionic skin with multi-modal sensing, broad-spectrum antimicrobial and regenerative capabilities for smart and expedited wound care, *Adv. Sci.* 8 (2021) 2004627, <https://doi.org/10.1002/advs.202004627>.
- [35] G. Shin, Y. Choi, B. Jeon, I. Choi, S. Song, Y.L. Park, Soft electromagnetic artificial muscles using high-density liquid-metal solenoid coils and bistable stretchable magnetic housings, *Adv. Funct. Mater.* 33 (2023) 2302895, <https://doi.org/10.1002/adfm.202302895>.
- [36] Y. Niu, G. Tian, C. Liang, T. Wang, X. Ma, G. Gong, D. Qi, Thermal-sinterable EGaIn nanoparticle inks for highly deformable bioelectrode arrays, *Adv. Healthcare Mater.* 12 (2023) 2202531, <https://doi.org/10.1002/adhm.202202531>.
- [37] S. Chen, H.Z. Wang, T.Y. Liu, J. Liu, Liquid metal smart materials toward soft robotics, *Adv. Intell. Syst.* 5 (2023) 2200375, <https://doi.org/10.1002/aisy.202200375>.
- [38] X. Chen, H. Wan, R. Guo, X. Wang, Y. Wang, C. Jiao, K. Sun, L. Hu, A double-layered liquid metal-based electrochemical sensing system on fabric as a wearable detector for glucose in sweat, *Microsyst. Nanoeng.* 8 (2022) 1–12, <https://doi.org/10.1038/s41378-022-00365-3>.
- [39] F. Han, R. Su, L. Teng, R. Xie, Q. Yu, Q. Li, Q. Tian, H. Li, J. Sun, Y. Zhang, M. Li, X. Liu, H. Ye, G. Li, G. Zhang, Z. Liu, Brittle-layer-tuned microcrack propagation for high-performance stretchable strain sensors, *J. Mater. Chem. C* 9 (2021) 7319–7327, <https://doi.org/10.1039/D1TC01598B>.
- [40] A. Ní Annaidh, K. Bruyère, M. Destrade, M.D. Gilchrist, M. Ottenio, Characterization of the anisotropic mechanical properties of excised human skin,

- J. Mech. Behav. Biomed. Mater. 5 (2012) 139–148, <https://doi.org/10.1016/j.jmbbm.2011.08.016>.
- [41] Q. Su, Q. Zou, Y. Li, Y. Chen, S. Teng, J.T. Kelleher, R. Nith, P. Cheng, N. Li, W. Liu, S. Dai, Y. Liu, A. Mazursky, J. Xu, L. Jin, P. Lopes, S. Wang, A stretchable and strain-unperturbed pressure sensor for motion interference-free tactile monitoring on skins, *Sci. Adv.* 7 (2021) eabi4563, <https://doi.org/10.1126/sciadv.abi4563>.
- [42] J. Liu, Z. Liu, X. Li, L. Zhu, G. Xu, Z. Chen, C. Cheng, Y. Lu, Q. Liu, Wireless, battery-free and wearable device for electrically controlled drug delivery: sodium salicylate released from bilayer polypyrrole by near-field communication on smartphone, *Biomed. Microdevices* 22 (2020) 53, <https://doi.org/10.1007/s10544-020-00511-6>.